Chemical Engineering Science, Vol. 46, No. 8, pp. 2055–2064, 1991.
Printed in Great Britain.

0009-2509/91 $3.00 + 0.00

THE MOTION OF TAYLOR BUBBLES IN VERTICAL TUBES—II. EXPERIMENTAL DATA AND SIMULATIONS FOR LAMINAR AND TURBULENT FLOW

ZAI-SHA MAO† and A. E. DUKLER‡
Department of Chemical Engineering, University of Houston, Houston, TX 77204-4792, U.S.A.

(*First received* 20 *January* 1989; *accepted in revised form* 26 *September* 1990)

Abstract The numerical method presented in Part I is used to simulate the liquid flow around a single Taylor bubble in a vertical tube. A modified low Reynolds number k–ε model is incorporated in the simulation for accurate prediction of the wall shear stress when liquid flow is turbulent. A model for free surface damping of turbulence is also included in the numerical process. The predicted rise velocity and the shape of the bubble as well as the film thickness and the wall shear stress are in good agreement with new experiments as well as earlier data.

INTRODUCTION

Gas–liquid slug flow (Fig. 1) is a flow pattern encountered when the two phases flow simultaneously upward in vertical tubes. This type of phase distribution is frequently observed in geothermal, oil and gas wells, reboilers, fermenters, process vaporizers and gas–liquid pipeline reactors. It also occurs during certain stages of the emergency core cooling of a nuclear reactor. Slug flow is characterized by the pseudo-periodic occurrence of large bullet shaped bubbles (designated here as Taylor bubbles) which occupy most of the cross-sectional area of the tube. The liquid moves upward as an aerated slug between two successive Taylor bubbles but flows downward in the form of a film around the Taylor bubbles. Fernandes *et al.* (1983) developed a detailed model for the characteristics of slug flow (slug and bubble lengths, pressure gradients and pulsation, residence time, holdup, backmixing, etc.), given the rise velocity of the individual Taylor bubbles. Predictions of heat transfer rates between the wall and the fluids and the mass transfer rates between the two fluids depend on this rise velocity and the shape of the Taylor bubbles. In the first paper in this series, Mao and Dukler (1990) developed a numerical algorithm for solving this free-surface problem when the flow is laminar (that paper is designated Paper 1). In the work that follows, the numerical method is extended to include the important practical cases where turbulent and transitional flow can take place. Also included is a treatment of the problem of damping of the turbulence near the solid boundaries and the free surface. Comparison is made with experimental data.

BACKGROUND

Stagnant liquid

Experimental and theoretical studies of a single Taylor bubble rising through stagnant liquid was reviewed in detail in Paper 1. The experimental results demonstrated that, for a wide range of viscosity and surface tension, the rise velocity can be expressed in terms of a constant Froude number:

$$Fr = \frac{U_N}{\sqrt{gD}} = \text{constant} \tag{1}$$

where D is the diameter of tube, and U_N is the rising velocity of the Taylor bubble. The shape of a Taylor bubble is spherical at the nose. Experiments by Harmathy (1960), Nicklin *et al.* (1962), White and

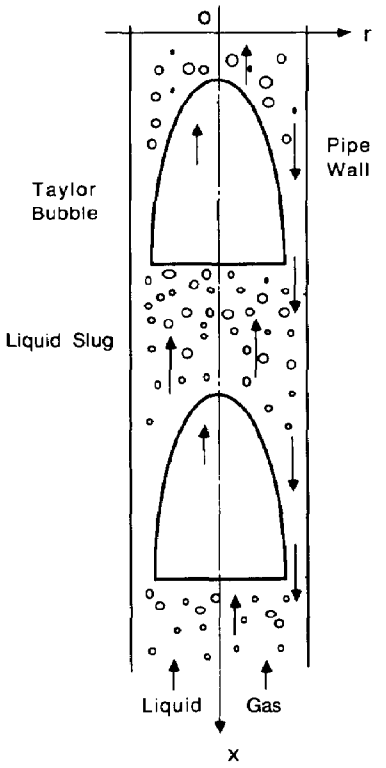

Fig. 1. Sketch of continuous slug flow.

†Present address: Institute of Chemical Metallurgy, Academia Sinica, Beijing, China.
‡Author to whom correspondence should be addressed.

Beardmore (1962), Zukoski (1966) and others all showed that $Fr = 0.35 \pm 0.05$. This constancy was observed over a fairly wide range of low viscosities and surface tensions. These results thus suggest that inertial forces control the rise velocity in stagnant liquids, and for this case potential flow theory can be applied.

Simplified theoretical approaches using potential flow were undertaken well before systematic experimental results were available. Dumitrescu (1943) proposed that the flow was potential around the nose of the bubble and that the nose was spherical in shape. In a coordinate system fixed on the bubble, the conditions of conservation of vorticity which exists for potential flow was used to find an approximate solution for this case of stagnant fluid by fixing the vorticity upstream as constant. Then he simply matched an approximate solution for potential flow around spherical surface and an asymptotic solution for an inviscid falling film with a common tangent at the junction on the surface to find the integration constant, and obtained an amazingly accurate result, $Fr = 0.351$. Surface tension was ignored. Davies and Taylor (1950) considered the potential flow around the bubble and truncated the theoretical Bessel function series solution for the stream function at only one term. A constant-pressure condition in the bubble was enforced at a point half of the tube radius along the bubble surface which led to a unique solution, $Fr = 0.328$. Recently, Bendiksen (1985) solved for the potential flow around a Taylor bubble in a tube including the effect of surface tension. He followed the procedures suggested by Dumitrescu (1943) but used additional terms in the series expansion for the stream function, arriving at a value of Fr not significantly different than that originally obtained by Dumitrescu.

Flowing liquid

In a flowing liquid the rising velocity of a Taylor bubble clearly must depend on the velocity of the liquid flowing upstream as well as on the rise due to buoyancy. Nicklin *et al.* (1962) investigated experimentally the velocity of a Taylor bubble in liquid flowing in a tube and suggested that the Taylor bubble velocity, U_N, can be expressed as

$$U_N = U_{NS} + cU_L \tag{2}$$

where U_{NS} is the translation velocity in stagnant liquid, U_L the average liquid velocity, and c is an empirical coefficient which varied widely as the direction and the speed of the liquid flow was changed. For upward flow at $Re > 8000$, $c = 1.2$, which suggests that the effective upstream velocity is the center line velocity of the liquid. Bendiksen (1984) did experiments in a vertical tube with flowing liquid, confirming that $c = 1.2$ in range of Re_L from 5000 to 110,000.

Collins *et al.* (1978) made measurements of U_N for a Taylor bubble in both flowing water and a glycerol solution. In approaching this problem theoretically, they followed Dumitrescu by solving the potential flow problem around the spherical nose. However, in their approach an upstream vorticity profile was selected to correspond to either the laminar or turbulent flow velocity profiles. They used the conditions for conservation of vorticity to find a solution to the problem of inviscid flow around the bubble in a flowing liquid, neglecting the effect of surface tension. Their analytical solution, which represents their measurements in turbulent flow quite well, is of the form

$$U_N = (gD)^{1/2}\phi + U_{LM} \tag{3}$$

$$\phi = Fr_L = U_{LM}/(gD)^{1/2}.$$

For flow with a turbulent velocity profile, they found that

$$U_N = U_{NS} + U_{LM} \tag{4}$$

was a good approximation to eq. (3), confirming the empirical eq. (2) for upward turbulent flow suggested by Nicklin *et al.* (1962). But eq. (4) is not valid for downward turbulent flow, casting doubt on the partition suggested by eq. (2). Collins' predictions for laminar flows failed to agree with the experimental data as well, probably because the viscous forces become important and the premise of vorticity conservation breaks down.

Few details are available concerning the flow in the falling liquid film around the bubble. Dumitrescu (1943) assumed it to be inviscid. Brown (1965) modified Dumitrescu's approach by assuming the film was in the equilibrium state that would be achieved under the combined forces of gravity and wall shear for laminar flow. Fernandes *et al.* (1983) and Orell and Rembrand (1986) similarly assumed that the film had reached equilibrium velocity but permitted turbulent flow conditions. Computational or experimental verification of these assumptions does not yet exist.

EXPERIMENTAL METHODS

These experiments on single Taylor bubbles were conducted in a vertical test column consisting of a plexiglass tube with 50.8 mm i.d. A measuring station was located 6.68 m above the inlet air nozzle where gas entered the column at the periphery through small holes and the water entered axially. This station was equipped with two pairs of conductance wires and a wall shear stress probe. The conductance wires were located 65 mm apart and used to measure the time variation of film thickness at the two locations and the velocity of the Taylor bubble from the cross correlation between the two signals. A double electrochemical probe located 3.0 mm above the lower wire probe and flush with the wall provided information on the magnitude and direction of the wall shear stress. Details on the design of the test section, the electronic circuitry and the calibration for individual probes are addressed by Mao and Dukler (1989)

Single Taylor bubbles were created in stagnant or upward flowing liquid by manually opening the gas

inlet valve to release a small amount of gas over a short time interval. The signals from the probes were recorded on analog tape and then digitized at 1 kHz frequency. A computer program was developed to process the data.

NUMERICAL METHODS

The numerical method used in this study is presented in detail in Paper 1. The method is developed there for a numerical solution of the full steady-state Navier–Stokes equation for a domain surrounding a Taylor bubble in a reference frame fixed on the rising Taylor bubble (Fig. 2). Our numerical task can be summarized as follows: with known diameter of tube, length of the Taylor bubble and physical properties of the fluid, compute the shape of the Taylor bubble, its translation velocity and the velocity at all positions in the liquid around the bubble. To this end, a program was developed based on the control volume formulation (Pantankar, 1980) using highly efficient discretizing algorithms specifically written for this type of computational domain and incorporating an algorithm for pressure and velocity correction. A new grid generation method is inroduced, designed to suit the curved surface of a Taylor bubble such that the specified boundary condition of interfacial shear and normal stresses can be enforced. All published solution methods include assumptions either as to the shape of the bubble or to a functional form for the shape. Because this constrains the nature of the solution the approach detailed in Paper 1 makes no such *a priori* assumptions.

When solving a case of laminar flow, initial velocity and pressure fields are specified along with an assumed initial shape of the bubble and the known boundary conditions. The fields for velocity components u and v are computed first and then the pressure correction is carried out sequentially in an iterative loop. All the discretized algebraic equation sets are solved by the Alternating Direction Implicit method with suitable relaxation. The shape is then adjusted by integrating a first-order differential equation to satisfy the balance of normal stress at the interface in order to maintain constant pressure inside the bubble. This process shows that multiple solutions can exist, a result consistent with the speculations of Garabedian (1957). A criterion is advanced for selecting the physically observed bubble. A physically realistic Taylor bubble must be symmetric and continuous at its vertex, and hence have a locally spherical nose. This procedure isolates a single computed rise velocity.

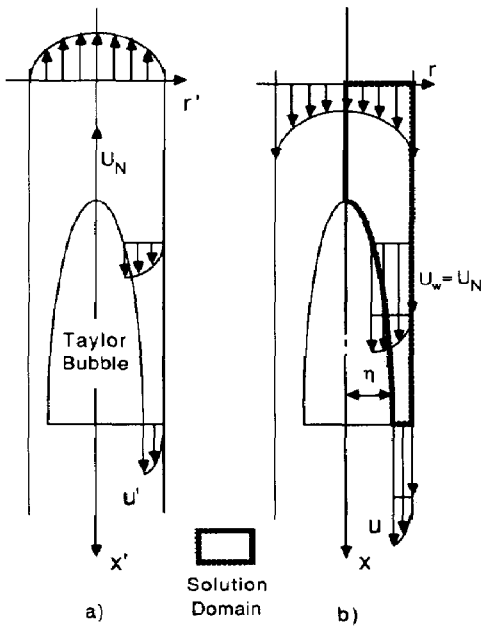

Fig. 2. A Taylor bubble rising in a vertical pipe: (a) in fixed coordinates, (b) in moving coordinates.

Turbulence model

Turbulence must be incorporated in the numerical program if the objective is to produce a model valid for practical flow rate ranges where Re is greater than the critical value of 2300. A convenient approach is the use of k–ε turbulence models where the effective viscosity μ_e replaces the molecular viscosity μ in the momentum equation and

$$\mu_e = \mu + \mu^t. \tag{5}$$

Such k–ε models are known to function well in situations where there is little or no circulation and these are precisely the conditions that exist upstream of the bubble and in the receding liquid film. Conditions below the bubble have little or no influence on the shape or rise velocity. The eddy viscosity μ^t is related to two transportable properties, the turbulent kinetic energy k and the energy dissipation ε (Jones and Launder, 1972, 1973):

$$\mu^t = c_\mu \rho \frac{k^2}{\varepsilon}. \tag{6}$$

where c_μ is one of a series of such coefficients incorporated in the model and determined from a series of experimental measurements. Therefore, in addition to the continuity and momentum equations for turbulent flow which now include the eddy viscosity, k and ε must be determined by their own equations. Conservation equations for these two quantities have been detailed in many publications including Launder and Spalding (1974) who give the recommended values for the coefficients suitable for locations removed from the damped viscous layer near the wall and for well-developed turbulence.

Modifications for low Re *and wall turbulence*

Many investigations have explored the adjustments needed to the k–ε model for application to regions near a solid boundary and for turbulent flow at low Re. All of these models propose exponential growth of the turbulent viscosity with distance to the wall in the

van Driest form. That is, the turbulent viscosity is multiplied by a factor of the form $[1 - \exp(-\eta y^+)]^2$. Here, y^+ is the dimensionless distance from the wall defined as $y^+ = yu^*/\nu$, where u^* is the friction velocity, y the distance from the wall, ν the kinematic viscosity, and η is a universal empirical constant.

Nagano and Hishida (1987) improved the Jones–Launder (1973) model by suitably modifying the conservation equations for k *and* ε, and showed that the model then works well in pipe flow for Re as low as 1835. While this equation provides the damping needed at the wall it remains deficient in that it permits a level of turbulence to exist even when Re drops below that for transition to laminar flow. Gill and Scher (1961) suggested a modification to the van Driest formula which handles this problem. Define

$$\Psi = \frac{y_m^+ - a}{b}$$

and the damping factor by $\{1 - \exp[-\Psi \backslash fy^+, y \backslash s(+, m)]\}^2$. Here $y \backslash s(+, m)$ is the maximum value of the dimensionless distance from the wall, i.e., its value at the axis of the tube. When a is chosen equal to y_m^+ at the transition Re, the quantity in brackets becomes zero as does the eddy viscosity at the transition Re. A value of $a = 60$ which corresponds to a transition Re of 1800 was used. $b = 26.5$ was recommended by Gill and Sher (1961).

The low-Re k–ε model of Nagano and Hishida (1987) revised to include the Gill–Scher coefficient as described above was incorporated into the solution algorithm and this was used for cases of turbulent flow. Details on the turbulent algorithm are provided by Mao (1988).

Turbulence model for the free surface

The free surface resembles a plane of symmetry for the velocity components as well as for k and $\tilde{\varepsilon}$, thus providing boundary conditions of zero normal gradient at the interface. But the free surface presents a limitation to turbulence in the normal direction so that the length scale is reduced and dissipation enhanced. The turbulent kinetic energy in the normal direction is also restrained. Thus, the free surface damps the turbulence as does a solid wall. Unfortunately, few investigations have been devoted to turbulence at a free surface. Ueda *et al.* (1977) and more recently Nezu and Rodi (1986) measured the eddy viscosity across the depth of an open channel and revealed a nearly parabolic distribution with zero values at both the solid floor and the free surface. In the absence of more definitive information, a damping model for the free surface is selected similar to that used at the wall in order to achieve similar distributions of turbulent viscosity as suggested from the measurements of Ueda *et al.* (1977). The following modification to the van Driest type damping factor is suggested which could be expected to be valid at any point between the wall and the interface of the falling film:

$$f_\mu = [1 - \exp(-\Psi y^+/26.5)]^2\,[1 - \exp(-z^+/\lambda)]^2 \tag{7}$$

where z^+ is the nondimensional distance from the interface. Boundary conditions at the free surface require zero gradients of k and $\tilde{\varepsilon}$ in the direction normal to the free surface.

For the free surface, the characteristic u^* used to calculate z^+ is the translation velocity of a Taylor bubble through stagnant liquid. When the tube diameter is small, the flow around a Taylor bubble is very quiescent and turbulence is less likely. The characteristic velocity u^* is small, so z^+ is small, and the damping of turbulence near the surface is large. With the benefit of some numerical experimentation it was found that the constant $\lambda = 600$ in eq. (7) generates a parabolic-like radial profile for effective viscosity in the film around a Taylor bubble, consistent with the experimental data mentioned above.

The numerical solution for the flow field can now proceed in a manner parallel to that for laminar flow as detailed in Paper 1 once appropriate values for the velocities as well and k *and* ε can be defined at the boundaries.

Specification of the turbulence parameters at the boundaries

At the wall the boundary conditions are $k = \varepsilon = 0$ while at the discharge plane of the domain the conditions must be chosen so that zero gradients in these turbulence characteristics exist in the flow direction. A fully established radial profile for k and ε must be prescribed at the inlet. For high Re, Nallasamy and Chen (1985) developed an empirical fit to the turbulent kinetic energy distribution data for pipe flow given by Hinze (1975). They also provided a fit to the distribution of the length scale, l_e, across the tube based on the data in Schlichting (1979), An inlet profile for ε when not experimentally available can be estimated by $\varepsilon = c_\mu \dfrac{k^{3/2}}{l_\varepsilon}$. Because the presence of the bubble itself can modify the flow upstream the computational domain including the bubble was placed after a development length of 3 m at the beginning of which the distribution of the turbulence parameters were specified from the fit to the data of Hinze and Schlichting.

A SINGLE TAYLOR BUBBLE IN STAGNANT LIQUID

Numerical simulation for low-viscosity liquids

Numerical simulations were carried out for single Taylor bubbles rising in stagnant liquid as a means of testing the methodology against well-established theoretical results. The results for bubbles rising in a 5 cm diameter vertical tube with $\mu = 0.001$ N s/m^2 and $\rho = 1000$ kg/m^3 appear in Table 1, case 1, where the flow is laminar but effects of surface tension are neglected. The criterion of a spherical shape at the nose was enforced to single out the unique rise velo-

city of the bubble. $Fr = 0.346$, the computed value, is in excellent agreement with the experiment. The predicted shape of the Taylor bubble close to the nose is plotted in Fig. 3, showing a good agreement with the profile derived from Dumitrescu's (1943) analytical solution. Computed velocity fields show the absence of circulation near the nose and the existence of downward flows near the wall well above the location of the bubble nose.

The predicted profiles of the film thickness h, wall shear stress τ_w, and saturation ratio, $\phi = \tau_w/\rho g h$, are shown in Fig. 4. For a film that has reached its equilibrium velocity and is no longer accelerating, $\phi = 1.0$.

Experimental results and comparison with prediction

Thirteen single Taylor bubbles were created in stagnant liquid. For each such bubble generated, the rise velocity and the film thickness around the bubble were obtained from conductance wire signals. The wall shear stress was measured simultaneously with the electrochemical probe. The rise velocity of an individual bubble was subject to inaccuracy attributed to the oscillation of the rising bubble around the center line and to the somewhat higher liquid velocity due to a small residual quantity of gas which entered the test column in the form of small bubbles in the wake of the Taylor bubble after the valve was closed.

The sample mean and standard deviation of these measurements of the rise velocity, after correction for bubble expansion during rise gave $U_N = 0.247 \pm 0.009$ m/s. In this system with the top open to atmosphere, the bubble expands as it rises, causing an apparent increase in velocity which can be calculated from

$$\Delta U_N = U_N \frac{\rho g l_{TB}}{p}$$

where U_N is the velocity that the bubble rises without expansion, and p is the pressure at the measuring station. The length of the Taylor bubble, l_{TB}, was measured during the experiments. The rise velocity computed from the numerical algorithm (Table 1, case 1) is thus is excellent agreement with the measurement.

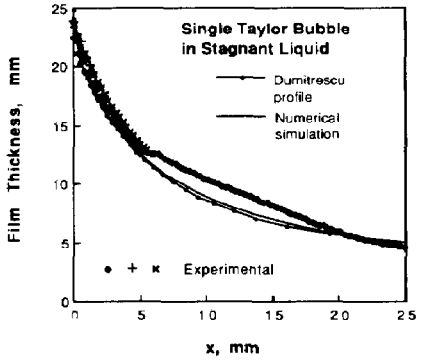

Fig. 3. Shape at the nose of a Taylor bubble. Comparison between measurement, numerical simulation and analytical prediction by Dumitrescu.

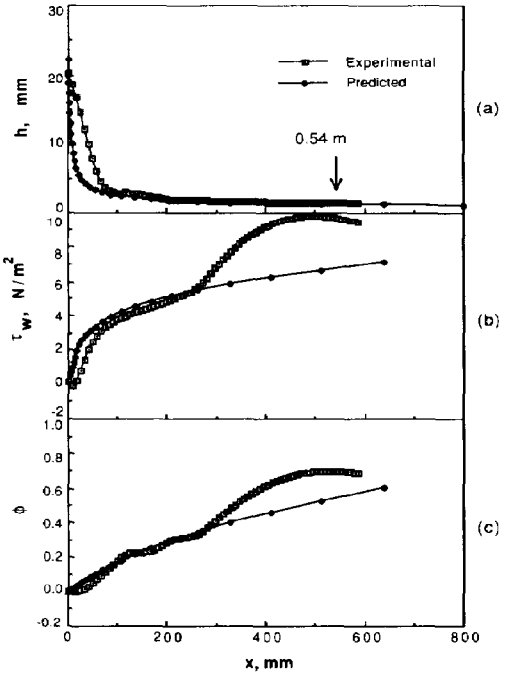

Fig. 4. Average profiles of film thickness, wall shear stress and saturation ratio for a collection of Taylor bubbles in stagnant liquid. The average length of the measured bubbles is indicated by an arrow.

Table 1. Computational results of Taylor bubbles in stagnant liquid

Case	μ (N s/m^2)	σ (N/m)	U_N (m/s)	Fr	r_N/R
1	0.001	0	0.242	0.346	0.715
2	0.001	0.075	0.2414	0.345	0.712
3	0.001	0.75	0.2388	0.341	0.636
4	0.005	0	0.2413	0.345	0.709
5	0.01	0	0.2392	0.342	0.704
6	0.05	0	0.2356	0.336	0.683

Typical time traces of film thickness, wall shear stress and the saturation ratio for a single Taylor bubble are shown in Fig. 5, where the arrival of the nose (indicated by marker A) and the bottom of the bubble (marker B) are indicated.

An enlarged plot of the traces for film thickness and wall stress as the lower part of the film passes appears in Fig. 6, showing the growth of surface roughness as the film recedes from the nose. By $t = 1350$ ms, a wavy structure of surface is evident. The frequency of large solitary waves is about 30 Hz, which is consistent with the range of wave frequency on a free falling film reported by Zabaras (1985). Correspondingly, the wall shear stress displays oscillation of increasing amplitude and of about the same frequency.

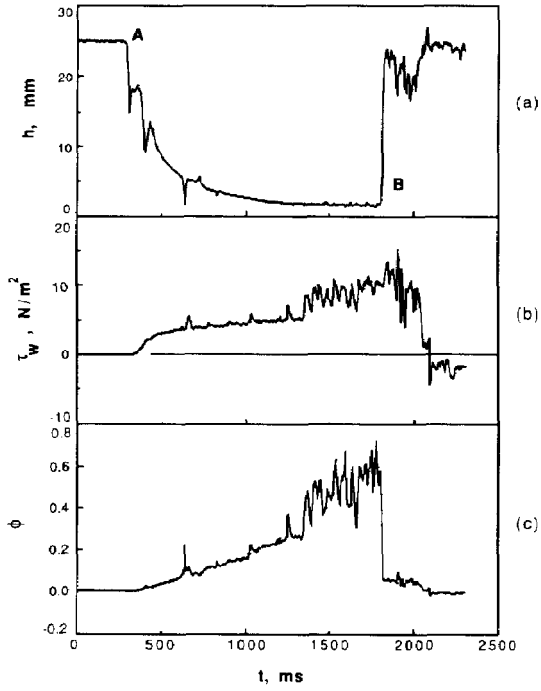

Fig. 5. Typical experimental profiles of film thickness, wall shear stress and saturation ratio for a Taylor bubble in stagnant liquid.

Two-wire probes with wires closely spaced can give erroneous reading when very thick liquid films moving at low velocities pass across the wires. As the top of the bubble first reaches the wires, the liquid bridge can persist for a few milliseconds if the velocity is low and thus gives false conductance readings. At higher liquid film velocities this does not take place (Zabaras, 1985). Evidence on the formation and drop-off of three such occurrences can be seen in the time traces of the film thickness in Fig. 5 at times less than 700 ms.

Traces such as those shown in Fig. 5 were obtained for all 13 bubbles and the ensemble of such traces for film thickness, wall stress and saturation ratio were fitted with cubic spline functions. The results appear in Fig. 4, where comparison with model predictions can be made. The film thickness is in good agreement past the location where surface tension effects cause erroneous readings for the reasons discussed above. The predicted saturation ratio and wall stress are in particularly good agreement with the experiment for the first 300 mm of distance along the film. Boundary layer calculations suggest that a transition to turbulent flow takes place at about this location. For these particular computations turbulence was not incorporated into the numerical model.

It is clear from these results that the film is still accelerating, not having reached its equilibrium thickness at the bottom of the bubble. In addition, the interface is very wavy. This new information will require modification of the model of Fernandes *et al.* (1983) which assumes saturation. Studies which extend the slug flow hydrodynamic model to heat and mass transfer will require this new information.

In only three of the Taylor bubbles was it possible to obtain clean information on the shape very near the bubble nose. In all other cases the appearance of random meniscus effects made this impossible. These three profiles are plotted in Fig. 3, where it is seen that near the nose the shape is in surprisingly good agreement with the Dumitrescu profile as predicted from the theory of potential flow.

In summary, these experimental results suggest that the Taylor bubble rising through stagnant liquid creates a developing free falling film around itself. Even for long bubbles the film at the bottom of the

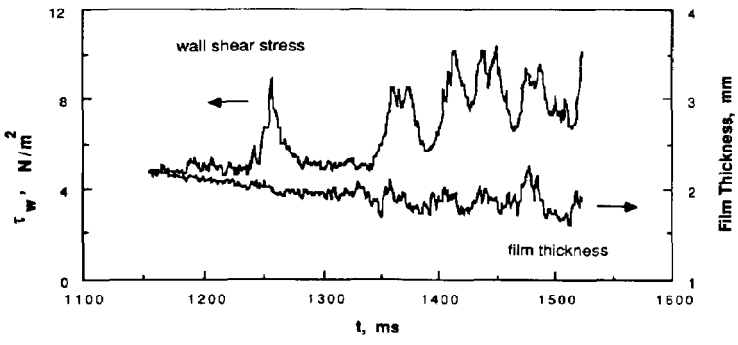

Fig. 6. Onset of turbulence in the falling film and the wavy structure at the free surface.

bubble is not yet in a state of equilibrium between the wall shear stress and the gravitational force. Along the wall a boundary layer develops and near the expected *Re* this boundary layer experiences a transition to turbulent flow. As the film develops behind the nose, the interface becomes wavy in a way similar to that observed for falling liquid films in the absence of interfacial shear.

Effects of surface tension and viscosity

In the presence of nonzero surface tension the pressure on the gas and liquid sides differ. Simulations were carried out with $\sigma = 0.075$ N/m and Fig. 7 shows the surface pressure profiles resulting. In the immediate vicinity of the nose, the sphericity generates a constant pressure difference due to surface tension. However, the effect on the rise velocity is very small as seen in Table 1, case 2. Even for a very large interfacial tension, $\sigma = 0.75$ N/m, the effect on the rise velocity continues to be small as is evident from Table 1, case 3. The effect of viscosity on the rise velocity is similarly discernable but small as shown by cases 4–6 in Table 1. Thus the computational results are in general accord with observation by White and Beardmore (1962) that, for low values of μ and σ, U_N is essentially independent of the physical properties of the liquid.

Computed film thickness profiles, wall stress, and saturation ratios, on the other hand, are strongly influenced by viscosity as shown in Figs 8–10. Thus, although changes in vicosity have little influence on the rise velocity of the bubble and on the resulting hydrodynamic model for slug flow they can be expected to play an important role in the modelling of the cognate transport processes.

A SINGLE TAYLOR BUBBLE IN FLOWING LIQUID

For a flowing liquid, the simulation requires input information on the radial distribution of velocity and, in the case of turbulent flow, the distribution of the turbulence parameters k and ε upstream of the nose of the bubble. Then the numerical procedure is executed with the value of U_N varied interactively according to the rules discussed in Paper 1 until the velocity is found at which the nose is locally spherical. Although these radial distributions are known for pipe flow, the effect of the presence of the bubble on their values is not known. To handle this problem a 3 m long section of pipe was added to the computational domain upstream of the bubble, the radial distributions specified upsteam and the computation allowed to proceed. The effect of the presence of the bubble on the velocity distribution is shown in Fig. 11 where the shape of the velocity profile which the bubble sees at its nose is significantly different from that far upstream. This result suggests that closely spaced Taylor bubbles can be expected to have different rise velocities than widely separated ones.

As an example of the results of such a simulation, the computed shape of the bubble near the nose (Fig. 12), the film thickness over the entire bubble [Fig.

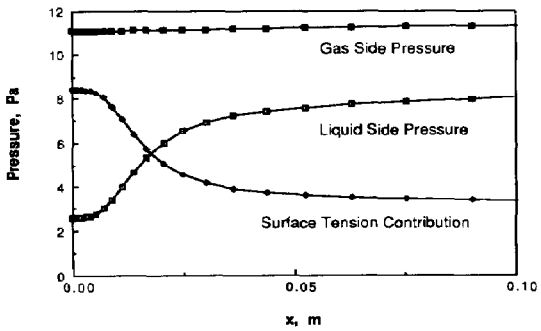

Fig. 7. Pressure profiles on both the gas side and the liquid side of the free surface and the surface tension contribution.

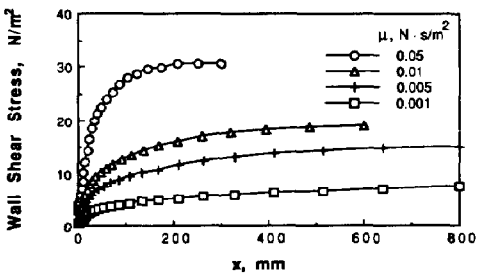

Fig. 9. Dependence of the profile of the wall shear stress on the liquid viscosity.

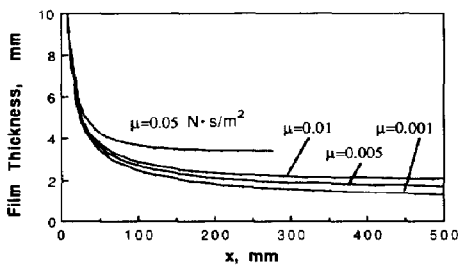

Fig. 8. Profiles of film thickness of a Taylor bubble in liquids with different viscosities.

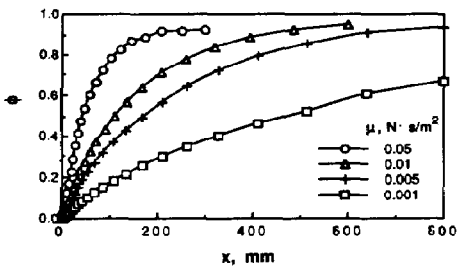

Fig. 10. Dependence of the saturation ratio on the viscosity of liquid.

13(a)] the wall shear stress along the film [Fig. 13(b)] and the saturation ratio [Fig. 13(c)] are compared with experimental data for nine bubbles generated in a flowing liquid to give a bubble rise velocity of 0.54 m/s. The computed shape near the nose is significantly different from that predicted by the Dumitrescu model, but in reasonable agreement with the measured shapes. Agreement between the theoretical predictions for film thickness, τ_w and ϕ, with the data-fitted cubic splines are reasonably satisfactory.

Comparison of simulations with experimental data of Collins for low-viscosity liquids and turbulent flow

Simulations were carried out for a range of flow rates from downward flow at $Re = 2500$ to upward flow at $Re = 10{,}000$ with fluid viscosity that of the Collins low-viscosity experiments. The excellent agreement between results of the simulation and the experiment appear in Fig. 14. The computation was also carried out with zero viscosity and no turbulence, and as Fig. 14 shows there is little influence of these properties on the results for high flow Re and low viscosities. Thus one can conclude that for these conditions the premise of Collins that the problem can be treated as one of potential flow is valid.

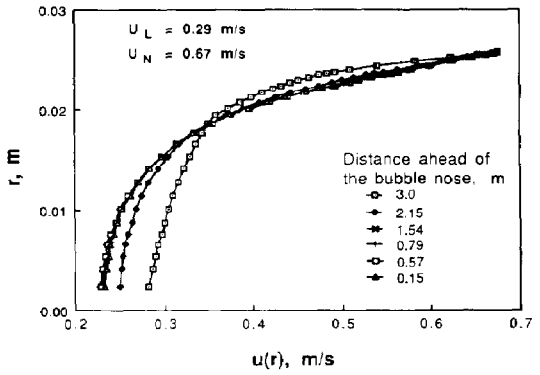

Fig. 11. Changes in velocity profile with approach to the nose of the bubble.

Comparison of simulations with experimental data of Collins for higher-viscosity liquids

Collins *et al.* (1978) assumed that the approach using potential flow would apply equally well at larger viscosities where the flow was laminar and the upstream profile was thus parabolic. They evolved two models, the results of which are expressed by the following two equations:

$$U_N = 2.27U_L + 0.361(gD)^{1/2} + \ldots \quad (8)$$

$$U_N = 2.16U_L + 0.347(gD)^{1/2} + \ldots \quad (9)$$

They also obtained experimental data for a glycerine–water solution ($\mu = 0.00582$ N s/m^2, $\rho = 1211$ kg/m^3) at a series of flow rates. Their data are compared with the theoretical models assuming inviscid flow but parabolic upstream velocity profile in Fig. 15. The deviations between theory and data were explained as due to an inadequate entry length and thus the failure to establish a full parabolic profile used in the theory.

Numerical simulations were carried out for liquid flow rates covered by the Collins experiments using a parabolic upstream profile and properties of the Collins glycerol solution experiments. Results of these simulations appear in Fig. 15 where excellent agreement between simulations and the experiment can be observed. The experimental point at the highest Fr_L which shows a small deviation from the prediction of the simulation was taken at a Re of 1850, just into the transition for turbulent flow. The slope of the line through the simulations yields a value of $c = 1.89$, in good agreement with the data of Nicklin *et al.* (1962) which indicated values of c ranging from 1.80 to 1.95.

Simulations were carried out corresponding to four experiments by Collins which clearly were in the transition and low-turbulence region. Because the full-turbulence model is invoked, including damping at the wall and the interface, this is a particularly severe test of the simulation. The very good agreement between predicted and simulated Fr for the bubbles is shown in Fig. 16. It thus becomes clear that a suitable model for the flow including a turbulence parameter

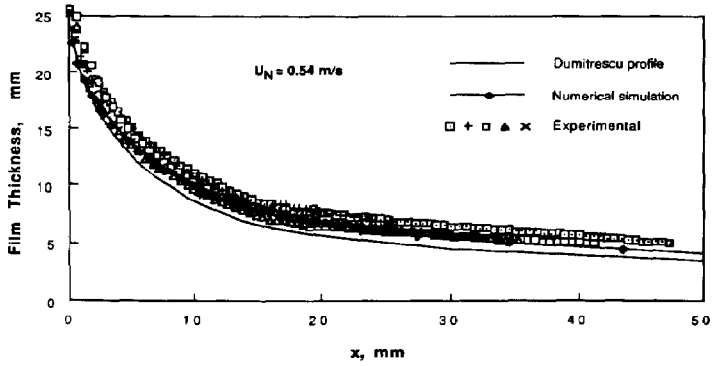

Fig. 12. Comparison of experimental shape profiles of the Taylor bubble with the Dumitrescu profile and the numerical simulation.

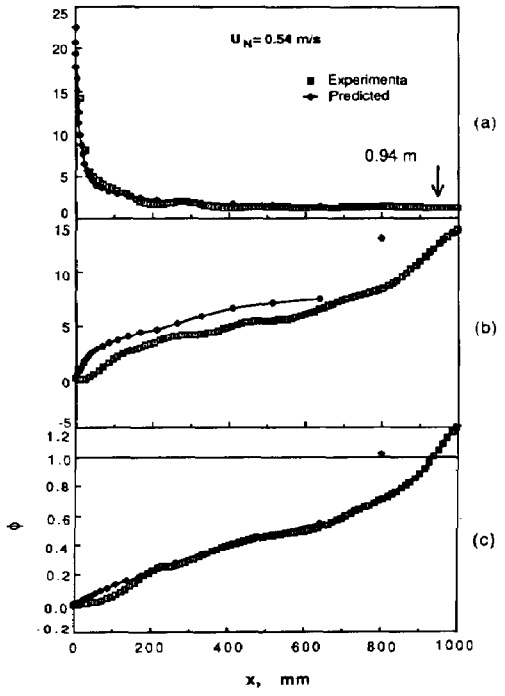

Fig. 13. Average profiles of film thickness, wall shear stress and saturation ratio for a group of Taylor bubbles rising at 0.54 m/s. Average length of the Taylor bubbles is indicated by an arrow.

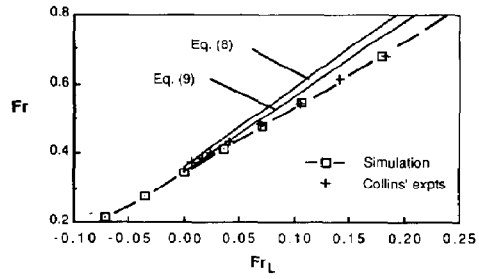

Fig. 15. Comparison of numerical simulation for parabolic profile with Collins' laminar flow data.

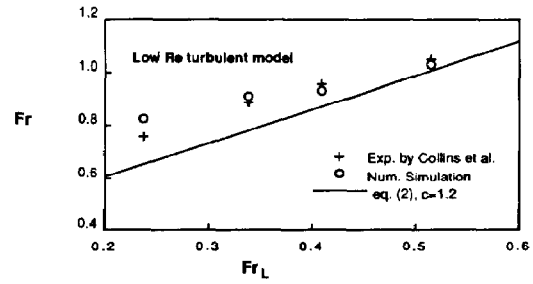

Fig. 16. Comparison of numerical simulation including full turbulence modelling with Collins' glycerol solution data for $Re > 1850$.

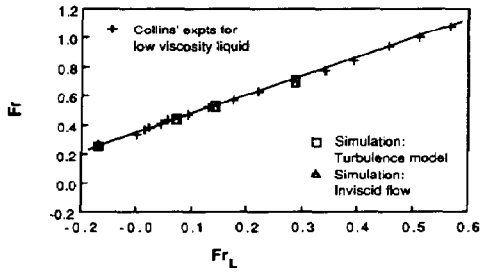

Fig. 14. Comparison of Collins' experimental data for water vs simulations using 1/7th power law for upstream velocity distribution.

when appropriate is necessary to evolve the correct upstream velocity distribution if the rise velocity is to be predicted with accuracy.

SUMMARY

The numerical method introduced in Paper 1 (Mao and Dukler, 1990) has been shown to reliably predict the flow surrounding a Taylor bubble. The criterion proposed for selecting a unique rise velocity from the array of multiple solutions appears to work. This eliminates the arbitrariness characteristic of all earlier studies where at least some characteristics of the bubble profile were specified ad hoc. The value of U_N for a single bubble is predicted accurately for both stagnant and flowing liquid. In addition, the evolution of the film thickness and wall shear stress with the axial distance appear to be predicted reliably. The film around the bubble is shown to continue to accelerate for long distances behind the nose in contrast to assumptions made earlier by others. The numerical simulation also correctly presents the influence of physical properties such as the viscosity and surface tension on the translation velocity and other characteristics of the flow. With a full numerical model in place extensions to problems of heat and mass transfer should be possible in a straightforward way.

Results from numerical simulations in this study suggest that the rise velocity of a Taylor bubble is essentially independent of viscosity and surface tension as suggested by Collins *et al.* (1978) for high *Re*. For laminar flow the approximation of constant vorticity is not satisfactory. The profile of the receding liquid film is critically dependent on the fluid properties, flow rates and turbulence levels, especially for flow rates near the conditions for transition between laminar and turbulent flow.

Acknowledgements—The financial support of the Shell Companies Foundation and the Schlumberger–Doll Research Co. is gratefully acknowledged.

NOTATION

c	coefficient defined by eq. (2)
D	pipe diameter; correction to the isotropic energy dissipation defined by eq. (17)
Fr	Froude number based on rise velocity of the bubble ($U_N/\sqrt{gD}$)
g	gravitational acceleration
h	film thickness
k	turbulent kinetic energy
l_{TB}	average length of Taylor bubbles in slug flow
r	radial coordinate
r_N	nose radius of a Taylor bubble
R	pipe radius
Re	Reynolds number ($U_L D/\nu$)
u	axial velocity component
u^*	friction velocity ($\sqrt{\tau_w/\rho}$)
U	average velocity
U_L	average velocity of upward liquid flow in tube
U_{LM}	center line velocity of flowing liquid
U_N	translation velocity of a Taylor bubble
U_{NS}	translation velocity of a single Taylor bubble in stagnant liquid
U_{SG}	superficial gas velocity of slug flow
x	axial coordinate
y	distance from the wall
y^+	dimensionless distance from the wall normalized with u^* and ν
z^+	dimensionless distance from the free surface

Greek letters

ε	rate of dissipation of turbulent kinetic energy
μ	viscosity
μ_e	effective viscocity
μ^t	eddy viscosity
ν	kinematic viscosity
ρ	density
σ	surface tension
τ	shear stress
ϕ	saturation ratio ($\tau_w/\rho gh$)

Subscripts

G	gas
L	liquid
w	wall

REFERENCES

Bendiksen, K. H., 1984, An experimental investigation of the motion of long bubbles in inclined tubes. *Int. J. Multiphase Flow* **10**, 467–483.

Bendiksen, K. H., 1985, On the motion of long bubbles in vertical tubes. *Int. J. Multiphase Flow* **11**, 797–812.

Brown, R. A. S., 1963, The mechanics of large gas bubbles in tubes: I. Bubble velocities in stagnant liquids. *Can J. chem. Engng* **56**, 75–82

Collins, R., De Moraes, F. F., Davidson, J. F. and Harrison, D., 1978, The motion of a large gas bubble rising through liquid flowing in a tube. *J. Fluid Mech.* **89**, 497–514.

Davies, R. M. and Taylor, G., 1950, The mechanics of large bubbles rising through extended liquids and through liquids in tubes. *Proc. R. Soc. Ser. A* **200**, 375–390.

Dumitrescu, D. T., 1943, Strömung an einer Luftblase im Senkrechten Rohr. *Z. angew. Math. Mech.* **23**, 139.

Fernandes, R. D., Semiat, R. and Dukler, A. E., 1983, A hydrodynamic model for gas–liquid slug flow in vertical tubes. *A.I.Ch.E. J.* **29**, 981–989.

Garabedian, P. R., 1957, On steady-state bubbles generated by Taylor instability. *Proc. R. Soc. Ser. A* **241**, 423–431.

Gill, W. D. and Scher, M., 1961, A modification of the momentum transport hypothesis. *A.I.Ch.E. J.* **7**, 61–63.

Harmathy, T. Z., 1960, Velocity of large drops and bubbles in media of infinite or restricted extent. *A.I.Ch.E. J.* **6**, 281–288.

Hinze, J. O., 1975, *Turbulence*. McGraw-Hill, New York.

Jones, W. P. and Launder, B. E., 1972, The prediction of laminarization with a two-equation model of turbulence. *Int. J. Heat Mass Transfer* **15**, 301–314.

Jones, W. P. and Launder, B. E., 1973, The calculation of low-Reynolds-number phenomena with a two-equation model of turbulence. *Int. J. Heat Mass Transfer* **16**, 1119–1130.

Launder, B. E. and Spalding, D. B., 1974, The numerical computation of turbulent flows. *Comput. Meth. appl. Mech. Engng* **3**, 269.

Mao, Z.-S., 1988, An investigation of two-phase gas–liquid slug flow. Ph.D. dissertation, University of Houston.

Mao, Z.-S. and Dukler, A. E., 1989, An experimental study of gas–liquid slug flow. *Exps Fluids* **8**, 169–182.

Mao, Z.-S. and Dukler, A. E., 1990, The motion of Taylor bubbles in vertical tubes, I. A numerical simulation for the shape and rise velocity of Taylor bubbles in stagnant and flowing liquid. In press.

Nagano, Y. and Hishida, M., 1987, Improved form of the k–ε model for wall turbulent shear flow. *J. Fluid Engng* **109**, 156–171.

Nallasamy, M. and Chen, C. P., 1985, Studies on effect of boundary conditions in confined turbulent flow predictions. NASA Contractor Report 3929.

Nezu, I. and Rodi, W., 1986, Open-channel flow measurements with a laser Doppler anemometer. *J. Hydraul. Div. Am. Soc. civ. Engrs* **112**, 335–355.

Nicklin, D. J., Wilkes, J. O. and Davidson, J. F., 1962, Two-phase flow in vertical tubes. *Trans. Instn chem. Engrs* **40**, 61–68.

Orell, A. and Rembrand, R., 1986, A model for gas–liquid slug flow in a vertical tube. *Ind. Engng Chem. Fundam.* **25**, 196–206.

Patankar, S. V., 1980, *Numerical Heat Transfer and Fluid Flow*. Hemisphere Press, Washington, DC.

Schlichting, H., 1979, *Boundary Layer Theory*. McGraw-Hill, New York.

Ueda, H., Möller, R., Komori, S. and Mizushina, T., 1977, Eddy diffusivity near the free surface of open channel flow. *Int. J. Heat Mass Transfer* **20**, 1127–1136.

White, E. T. and Beardmore, R. H., 1962, The velocity of rise of single cylindrical air bubbles through liquids contained in vertical tubes. *Chem. Engng Sci.* **17**, 351–361.

Zabaras, G. J., 1985, Studies of vertical annular gas–liquid flows. Ph.D. dissertation, University of Houston.

Zukoshi, E. E., 1966, Influence of viscosity, surface tension, and inclination angle on motion of long bubbles in closed tubes. *J. Fluid Mech.* **25**, 821–837.